



Depth profile of a time-reversal focus in an elastic solid



Marcel C. Remillieux^{a,*}, Brian E. Anderson^a, T.J. Ulrich^a, Pierre-Yves Le Bas^a, Cedric Payan^b

^aGeophysics Group (EES-17), MS D446, Los Alamos National Laboratory, Los Alamos, NM 87545, United States

^bAix Marseille Université, Laboratory of Mechanics and Acoustics, LMA CNRS UPR 7051, 31 chemin Joseph-Aiguier, 13402 Marseille CEDEX 20, France

ARTICLE INFO

Article history:

Received 26 August 2014

Received in revised form 12 December 2014

Accepted 13 December 2014

Available online 24 December 2014

Keywords:

Time-reversal

Elastodynamics

Lamb's problem

ABSTRACT

The out-of-plane velocity component is focused on the flat surface of an isotropic solid sample using the principle of time reversal. This experiment is often reproduced in the context of nondestructive testing for imaging features near the surface of the sample. However, it is not clear how deep the focus extends into the bulk of the sample and what its profile is. In this paper, this question is answered using both numerical simulations and experimental data. The profiles of the foci are expressed in terms of the wavelengths of the dominant waves, based on the interpretation of the Lamb's problem and the use of the diffraction limit.

Published by Elsevier B.V.

1. Introduction

Over the last decade, a number of sophisticated imaging techniques have emerged that combine the properties of nonlinear elasticity observed in a damaged material and the principle of time reversal (TR) [1–7]. A TR mirror (TRM) allows focusing narrowly energy in space and time. If energy is focused near a damaged region (e.g. crack, delamination), the relatively large amplitude of the wave field at that location will activate a nonlinear elastic response in the test sample, which can then be exploited for imaging applications.

A standard TR experiment in a reverberant elastic medium is a two-step process [8]. In the first step, or *forward* propagation, a known signal is emitted from a transducer (source) at a point *A* on the surface of the sample while another transducer (receiver) records the response at a point *B* on the surface. The received signal is the convolution of the source signal with the impulse response between the source transducer at *A* and receiver transducer at *B*. This impulse response is rather complex due to the multiple paths (e.g. reflections) that the waves may follow within the bounded medium. In the second step, or *backward* propagation, the received signal is reversed in time and emitted from the transducer at point *B*. As a result of the invariance of the TR operator in a lossless medium [9], the elastic wave field focuses on point *A* and reconstructs the original source signal. There are some imperfections in this reconstruction process, mainly because the directional information of the energy

received in the *forward* signals is typically not used, attenuation that exists in a realistic system, and because a limited (as opposed to infinite) acquisition time of the *forward* propagation signal is available. An alternative to standard TR is reciprocal TR (R-TR) [10–12]. In R-TR, the reversed signal is emitted from the original source position *A* and the elastic wave field focuses at the original receiver position *B*. It is possible to interchange the source and receiver positions thanks to the principle of spatial reciprocity [13].

In the context of a TR experiment, a reverberant medium offers a number of advantages over an unbounded one. In an unbounded homogeneous medium, the TRM ideally forms a closed surface around the source [14]. In practice, however, the TRM often has a small aperture and does not capture the full wave field propagating away from the source, which leads to an imperfect reconstruction of the focused signal [15]. In contrast, the multiple reflections of the waves on the boundaries of a medium with a finite size act as virtual sources that improve the quality of the TR focusing. Therefore, if the modal density within the finite medium is sufficiently large and damping is relatively small, the TRM can be reduced to a single element. Following this idea, a number of TR experiments have been conducted using *chaotic cavities* [16–18], where one emitter is used within a cavity of arbitrary shape. Such devices will enhance wave scattering and break any symmetry that could potentially exist in the problem. In this paper, the cavity has the shape of a rectangular parallelepiped, so multiple transducers must be used to break the symmetry of the problem.

TR of elastic waves in a solid is a more complex problem than TR of acoustic waves in a fluid because the wave field is no longer scalar but vectorial. Consequently, different types of wave motions

* Corresponding author.

E-mail address: mcr1@lanl.gov (M.C. Remillieux).

may coexist in a solid: e.g. shear (S), compressional (P), and Rayleigh (R) waves. Draeger et al. [19] delineated theoretically the mechanisms involved in the focusing of P and S waves in a solid half-space using a TRM. A point source in the solid generated P and S waves, which propagated to a TRM placed in a fluid surrounding the solid. In the far-field, the P and S waves separate because of their different propagation speeds and reach the TRM at different times. This property may be used to focus the P and S waves in the solid, almost independently from one another. It was shown that when the signals from both waves are emitted by the TRM into the fluid, each wave generates a P and an S wave in the solid, thus leading to a total of four waves propagating in the solid. Two of these waves will focus properly, while the other two will not and simply generate some “low-level noise”. In experiments, Draeger et al. [20] related the size of the focal spot to the type of wave used in the TR process and validated their theoretical analysis. Sutin et al. [12] designed a TR experiments in a reverberant solid sample using only one transducer. They successfully focused elastic energy on the surface of the sample using the out-of-plane velocity component at the selected focal point where the receiver was placed. They reported that the width of the focal spot at -3 dB was equal to a factor $\times 0.44$ of the shear wavelength at the center frequency of the pulse for a doped-glass block, which is a weakly dissipative medium. In fact, if the reference wave is taken as the Rayleigh wave, then they reach exactly the diffraction limit. Ulrich et al. [21] showed in a series of R-TR experiments and simulations that a scalar source (or a source whose radiation characteristics are not known) may be used to focus selectively vector components of the motion (either individual components or some combinations of them) on the surface of a sample. For instance, if energy is focused at a point on the surface of the sample using the out-of-plane velocity component, the in-plane components of the velocity vector will exhibit amplitude levels that are similar to the temporal side lobes of the reconstructed pulse, i.e. “low-level noise”. However, in their study, they did not relate the size of the focal spot to the types of waves propagating in the medium. In most TR experiments it is not possible to probe the elastic wave field in the bulk of the sample. Numerical simulations are an alternative to experiments when the wave propagation needs to be characterized within the bulk of the sample. Some recent work involving simulations of TR experiments in solids have been carried out but were limited to 2D systems [22,23], thus possibly missing some features that could be observed in a realistic 3D system.

In this paper, the out-of-plane velocity component is focused on the surface of a 3D aluminum sample using R-TR. The focal spot has a finite size related to the types of waves propagating within the medium and to the center frequency of the focused signal (e.g. pulse). The focal spot observed in experiments on the surface of a sample also extends into the bulk of the sample with an unknown depth profile. In this context, the objective of this paper is to characterize the depth profile of the TR focal spot for various conditions (e.g. center frequencies and material properties). In the context of nondestructive testing (NDT), this profile relates to the portion of a sample that will be probed around the focal time of a TR experiment and consequently to the nonlinear signature that will be recorded. Since depth profiles of the TR foci cannot be measured experimentally, the analysis is supported mainly by numerical simulations, within the framework of linear elasticity. Experimental data are used mainly to validate the numerical model. The paper is organized as follows. Section II validates the numerical model used in the rest of the analysis against experimental data for the case where elastic energy is focused near an edge of an aluminum block. Section III examines the depth profiles of the TR foci on a surface of a block for various material properties and center frequencies of the focused signal. Section IV concludes.

2. Experimental validation of the numerical model

2.1. Experiments

Experiments were conducted on an aluminum sample with a rectangular shape and dimensions of $10 \times 10 \times 19$ cm³. Fig. 1 is a photograph of the experimental setup. Elastic energy was transmitted into the sample using eight identical piezoelectric disks (type PZT-5, diameter of 12.7 mm, and thickness of 2 mm) that were glued onto three surfaces, at locations far from the desired focal point to allow diffusion of the elastic energy into the sample. The velocity wave field was measured on the surface of the sample using single point laser Doppler vibrometers (LDV) from Polytec Inc. The normal component of the velocity was measured with the OFV 303 (3001 controller, VD-02, 5 mm/s/V) and the in-plane components with the OFV 552 (5000 controller, VD-02, 5 mm/s/V) fiber-optic differential laser vibrometer. The angle of $\pm 30^\circ$ between the fiber-optic laser heads and the surface normal is used to eliminate the normal component of the velocity vector through subtraction and provide the in-plane component [24]. A rotation stage is incorporated to allow measurements in the two orthogonal in-plane directions of motion when the fiber-optic laser heads are rotated 90 degrees. Source signals were generated with an 8-channel, 12-bit A/D Gage CompuGen 8150 card and received signals were digitized with a 2-channel, 14-bit D/A Gage CompuScope 14,200 cards using a sampling rate of 10 MHz per channel. Source signals were amplified 50 times with Tegam 2350 power amplifiers. A scanning system was developed that allows the laser vibrometer to record the motion of the sample at various locations within a region of interest with a system consisting of a Newport ESP300 positioning controller and two Newport ILS250MVTP linear-axis translation stages that move the laser and pause during the measurement at each scan point location. The experiment was setup on a floating, vibration isolation table (Newport LW3048B).

The R-TR method [8] is used to create a focus of the vertical, in-plane component of motion centered at the location of the laser spot in Fig. 1 (point B). First, impulse responses (IRs) are determined between the PZT transducers and point B . For this purpose, a linear chirp signal with appropriate frequency bandwidth is emitted from a single PZT transducer while the vertical, in-plane velocity component is measured with the LDV at point B . This operation is repeated for all PZT transducers. Then, the IRs are determined from a cross correlation of the input chirp signal with the measured response, reversed in time, scaled in amplitude to maximize the amplifier output, and all reversed signals are broadcast simultaneously from the corresponding PZT transducers. This creates a TR focus of the vertical, in-plane velocity component (v_z). The in-plane velocity component (v_x) and the out-of-plane velocity component (v_y), are also measured. Spatial scans of the TR focus in each component of motion are displayed in Fig. 2.

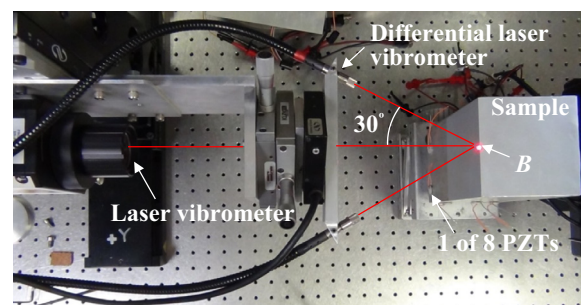


Fig. 1. Photograph of the experimental setup.

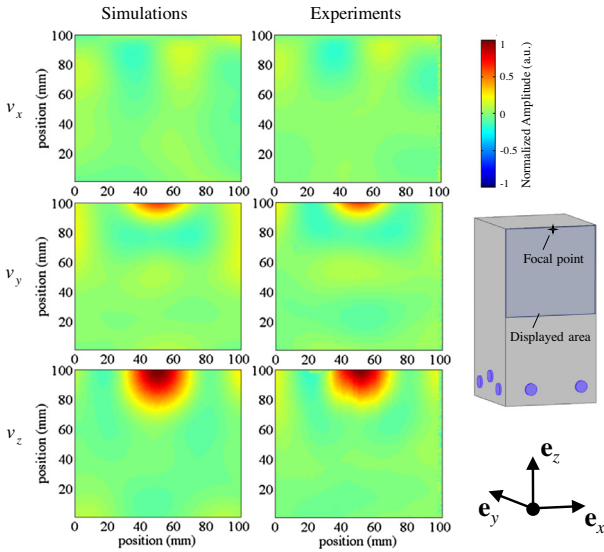


Fig. 2. Velocity components at the focal time. Focusing was achieved using the v_z component at the focal point. The drawing on the right-hand side indicates the location of the focal point and the area on the sample surface where results are displayed. Simulated (left column) and experimental (right column) results. For each column, data are normalized with respect to the peak amplitude of v_z . The v_z signal generated at the focal point (see Fig. 3) consists of a pulse centered at 52.8 kHz in simulations and at 54.7 kHz in experiments. As a result, the spot size of v_z is larger in simulations than in experiments. Witness the dipole motion around the focal point observed in v_x due to the Poisson effect. This motion has a much smaller amplitude than v_z at the focal point but is larger than the background.

2.2. Numerical model

The above experiment is simulated using the “Solid Mechanics” module of the commercial finite-element software package COMSOL MULTIPHYSICS 4.3a. In the simulations, the aluminum has a mass density of 2700 kg m^{-3} , a Young’s modulus of 70 GPa, and a Poisson’s ratio of 0.33. The PZT transducers are not modeled. Instead, a normal surface load is applied at the location of the transducers. The time history of the surface load in the forward-propagation step consists of a 50 kHz tone-burst with a full bandwidth at half maximum (FBHM) of 10 kHz, similar to that observed in the experiments at the focal point. The computational domain is discretized into quadratic tetrahedral elements with a maximum size of 5 mm, which corresponds to 10 elements per smallest wavelength at 55 kHz (center frequency + half bandwidth of the pulse). The smallest wavelength is that of the Rayleigh wave and is equal to 52.9 mm, based on a propagation speed of 2910 m.s^{-1} . Transient simulations are carried out using a time step of $0.1 \mu\text{s}$, which satisfies the Courant–Friedrichs–Lewy condition for a 3D problem of elastodynamics.

2.3. Discussion

Fig. 2 depicts snapshots of the three simulated and measured velocity components, v_x , v_y , and v_z , at the focal time of $t = 1.876 \text{ ms}$. Results are displayed on a portion of the surface surrounding the focal point. Time histories of these velocity components at the focal point are shown in Fig. 3. The v_z component exhibits the largest peak amplitude at the focal time, which is expected since this is the component used in the TR process. A significant portion of the elastic energy is also contained in the y -component of the motion, as a result of focusing near an edge parallel to the x -axis. The asymmetry of the system in the y -direction (e.g. fluid or vacuum on one side of the focal point and solid on the other side) causes motion of the focal-point region in the y - z plane.

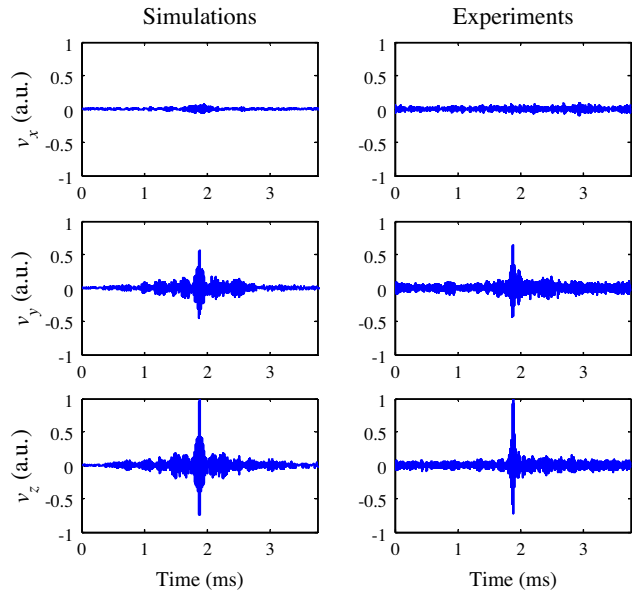


Fig. 3. Time histories of the velocity components at the focal point, for the problem settings described in Fig. 2. Simulated (left column) and experimental (right column) results. For each column, data are normalized with respect to the peak amplitude of v_z .

Likewise, if the focal point was close to a corner of the sample, energy would be contained in all three components of the motion, regardless of the component used in the TR process, due to the asymmetry of the system in the three Cartesian directions. Last, it is interesting to observe the dipole structure of the v_x component around the focal point, due to the Poisson effect. This motion has much smaller amplitude than v_z at the focal point but is larger than the background.

The numerical model captures successfully the main features of the elastic response observed in experiments, including the dipole structure of the v_x component and the focal spots for the v_y and v_z components in Fig. 2. Note that the size of the focal spot for the v_z component is larger in simulations than in experiments. As discussed in the introduction, the size of the focal spot is related to the center frequency of the focused signal at the focal point. The signal of the v_z component at the focal point consists of a pulse centered at 52.8 kHz in simulations and 54.7 kHz in experiments, which implies a smaller size of the focal spot in experiments. It is also worth mentioning that, in Fig. 3, the ratios between the peak amplitudes of the v_y and v_z components at the focal point are 57% in simulations and 63% in experiments. The close qualitative and quantitative agreements between experiments and simulations are remarkable given the different approaches used to create the TR signals.

3. Focusing elastic energy at the center of a flat surface

The out-of-plane velocity component (now v_z) is focused numerically at the center of the top surface of the aluminum sample described in Section 2. A Ricker wavelet is used in the forward-propagation step of the TR simulation. This pulse has a wider bandwidth than that described in Section 2.2, and thus will lead to a focusing of better quality. For instance, a Ricker pulse centered at 50 kHz has a FBHM of nearly 58 kHz. Besides, the fact that Ricker wavelets are commonly used in the field of elastodynamics makes the study more general than using a narrowband pulse mimicking a particular experiment. The computational domain is discretized with at least 6 quadratic tetrahedral elements per smallest wave-

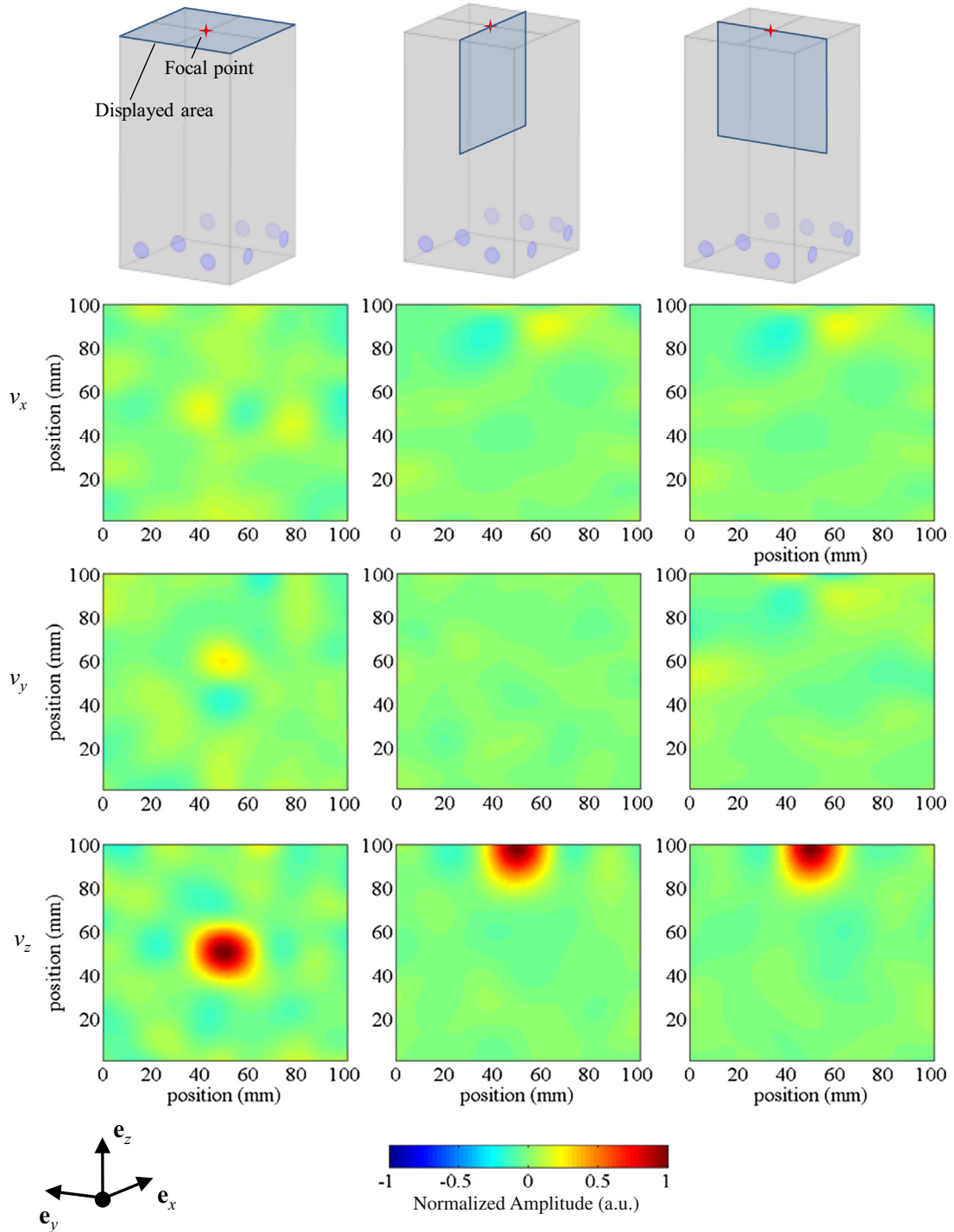


Fig. 4. Simulated velocity components at the focal time. Focusing was achieved using the v_z component. The drawings on the bottom row indicate the location of the focal point and the area where results are displayed. Data are normalized with respect to the peak amplitude of v_z . The v_z signal generated at the focal point consists of a pulse centered at 79.2 kHz.

length. For a Ricker wavelet centered at 50 kHz, the maximum element size is set to 5 mm (the same mesh is used in Section 2.2).

Snapshots of the three simulated velocity components at the focal time are depicted in Fig. 4, for a pulse centered at 79.2 kHz. Results are displayed on the top surface (x - y plane) and within the depth of the sample (x - z and y - z planes). As expected, the largest amplitude is observed for the v_z component while the in-plane components, v_x and v_y , exhibit the Poisson effect (dipole structure) discussed in Section II. The focus has the shape of a half prolate

spheroid, elongated along the z -axis. It is not perfectly symmetric with respect to the z -axis, indicating an imperfect reconstruction of the original source. The normalized surface and depth profiles of the focus are shown in Fig. 5. Their respective size can be analyzed in connection with Lamb's problem described below.

Fig. 6 shows snapshots of the v_x and v_z components in the x - z plane due to a normal point load on the surface of a larger aluminum sample with dimensions of $0.4 \times 0.2 \times 0.2 \text{ m}^3$. This is a forward-propagation problem that does not involve TR. The load

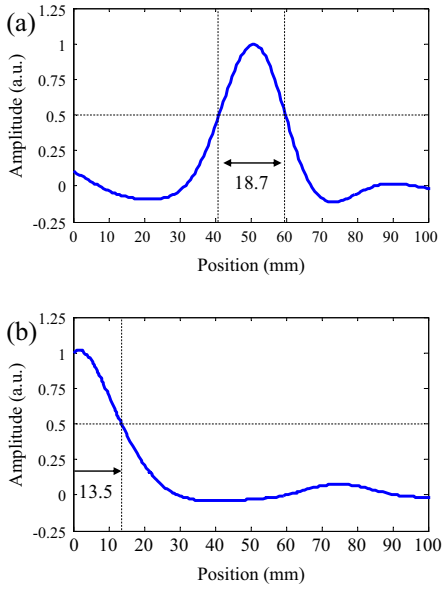


Fig. 5. Simulated surface and depth profiles of v_z at the focal time. The v_z signal generated at the focal point consists of a pulse centered at 79.2 kHz.

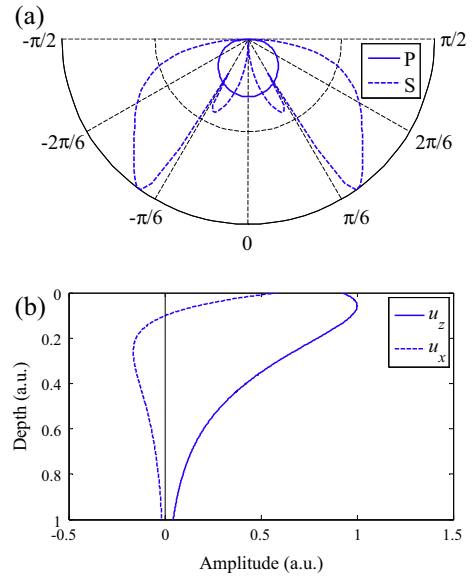


Fig. 7. Analytical far-field radiation patterns in an elastic half space for Lamb's normal point load problem in 3D. (a) P and S waves. (b) Vertical and horizontal motion components of the R wave. Note that the peak amplitude of the Rayleigh wave is found beneath the surface, which is consistent with the depth profile of the TR focus in Fig. 5.

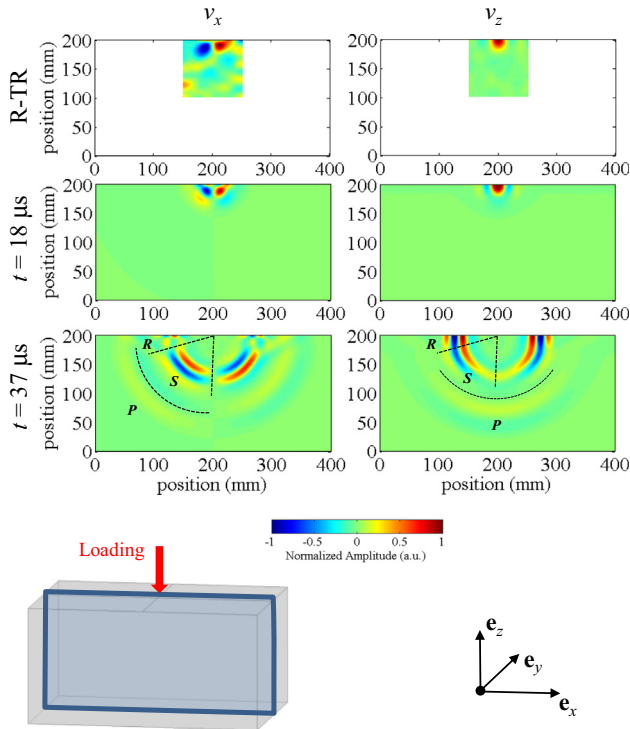


Fig. 6. Simulated velocity components in the near and mid fields due to a normal point load applied on the surface of the sample (*forward-propagation* problem). The two plots on the top row are the velocity components at the focal time of the corresponding R-TR problem, reproduced here for convenience. For each plot, data are normalized with respect to the peak amplitude of the corresponding velocity component. The time history of the load is a Ricker wavelet centered at 75 kHz.

signal consists of a Ricker wavelet centered at 75 kHz. Results are displayed at times $t = 17 \mu\text{s}$ (near-field radiation) and $37 \mu\text{s}$ (mid-field radiation). For convenience, the v_x and v_z components at the focal time of the R-TR simulation (see center column in Fig. 4) are scaled appropriately and reproduced in this figure (top row).

This *forward-propagation* problem would be equivalent to Lamb's normal point load problem [25] if the medium was an elastic half space. Analytical solutions have been derived for this problem but are mostly limited to the far-field radiation [26,27], as shown in Fig. 7 for a harmonic, point-load (3D) configuration. Most of the features of the far-field radiation can also be observed in the mid-field: (i) S waves dominate the elastic wave field in the bulk of the sample, with their amplitude being the largest between the angles of $\pi/6$ and $2\pi/6$ with respect to the vertical axis; (ii) the vertical component of the R wave reaches a maximum beneath the surface while its horizontal component experiences a phase change along the depth. The R -wave features are also observed in the vertical and horizontal components of the velocity field at the focal time of the TR simulation indicating that R waves dominate the propagation in the vicinity of the surface in a TR experiment. This would explain why the peak amplitude of the focal spot in Fig. 5 is not found exactly on the surface (where the velocity component is focused) but beneath it. Last, it is interesting to observe that the R-TR process recreates an approximate snapshot of the near-field *forward* radiation. The size of the virtual source is controlled by the diffraction limit, thus preventing the reconstruction of details smaller than the wavelength(s) of the wave(s) involved in the propagation.

In a perfect TR experiment, the diameter of a focal spot measured at the half maximum value is equal to one half of the dominant wavelength, as a consequence of the diffraction limit. On the surface of the sample, the propagation is dominated by the R waves. Therefore, the diameter of the focal spot in the x - y plane can be expressed as,

$$w^{\text{emp}} = \lambda_R/2, \quad (1)$$

where the superscript "emp" refers to empirical. Along the z -axis, the propagation is dominated by R waves close to the surface and S waves in the bulk of the sample. As a result, the focal spot in a vertical plane of the sample has the shape of a half ellipse. Although two types of waves dominate the propagation, their wavelengths

Table 1

Measured and simulated sizes (width and depth) of the focal spot during the TR focusing of the out-of-plane motion component (v_z) for various materials and center frequencies of the focused signals.

Data type	Material	E (GPa)	ν	ρ (kg m ⁻³)	f_c (kHz)	λ_p (mm)	λ_S (mm)	λ_R (mm)	w^{obs} (mm)	w^{emp} (mm)	d^{obs} (mm)	d^{emp} (mm)
Num	Aluminum	70	0.33	2700	53.4	116.1	58.5	54.5	28	27.3 (-2.5%)	19.2	19 (-1%)
Num	Aluminum	70	0.33	2700	79.2	78.3	39.4	36.7	18.7	18.4 (-1.6%)	13.5	12.8 (-5.2%)
Num	Undefined	70	0.15	2700	59.2	88.4	56.7	51.2	26	25.6 (-1.5%)	19.2	18.4 (-4.2%)
Num	Undefined	70	0.2	2700	59.4	90.4	55.3	50.4	25.6	25.2 (-1.6%)	18.8	18 (-4.3%)
Num	Undefined	70	0.45	2700	55	180	54.4	51.5	26	25.8 (-0.8%)	17.8	17.7 (-0.6%)
Exp	Aluminum	/	/	2705	75	83.4	42	39.2	20.1	19.6 (-2.5%)	/	/
Exp	Aluminum	/	/	2705	123	50.9	25.6	23.9	12.3	12 (-2.4%)	/	/
Exp	Aluminum	/	/	2705	152	41.2	20.7	19.3	10.2	9.7 (-4.9%)	/	/
Exp	Aluminum	/	/	2705	169	37	18.7	17.4	8.9	8.7 (-2.2%)	/	/

are proportional to one another so that the depth of the focus can be expressed in terms of one wavelength only as,

$$d^{emp} = 1.3\lambda_S/4, \quad (2)$$

where the factor 1/4 is assumed because the diffraction-limit theory is applied to a half focal spot and the factor 1.3 is found by inspecting the radii of the focal spots in the z -direction for all the numerical simulations.

Results from simulations and experiments for various material properties and center frequencies of the focused signals are summarized in Table 1. Material properties were those of aluminum but with a Poisson's ratio varied from 0.15 to 0.45. Center frequencies were varied from 53 to 169 kHz. There is a fair agreement between the observed and predicted sizes of the focal spots, with differences mostly within 5% for all cases considered. Besides the use of an empirical expression, variations of the results can be attributed to the imperfect reconstruction of the source in the R-TR process. Note that an expression of d^{emp} involving λ_p would not be robust to changes of the Poisson's ratio. This is another indication that in the bulk of the sample, the diffuse wave field is mostly dominated by S waves.

Before closing this section, some important differences between 2D and 3D modeling are outlined in the context of TR near the surface of an elastic solid. The volumetric strain is chosen for the analysis since it has been used in previous numerical work related to imaging applications where the principle of TR is combined with the properties of nonlinear elasticity [23]. The volumetric strain is an eigenvector of the elasticity tensor and thus can be used to apply scalar nonlinearity laws in which, for instance, the volumetric stiffness is a power series of the volumetric strain. The volumetric strains obtained at the focal time of a TR experiment simulated with 2D and 3D models are shown in Fig. 8. In both simulations, a Ricker wavelet centered at 75 kHz was used in the *forward-propa-*

gation problem and the out-of-plane velocity component was focused. In 2D, the volumetric strain has a pear-like shape, which was also predicted by Janssen and Van Den Abeele [23]. It reaches two local maxima, one close to the surface where the R waves dominate and one in the bulk of the sample where the P and S waves dominate. In 3D, the volumetric strain field has the shape of a half ellipse with only one local maximum obtained on the surface of the sample and a penetration depth of only 5.3 mm, for the case of a pulse centered at 75 kHz. In this case, the depth profile of the volumetric strain seems to be dominated by the R waves only, which decay exponentially with depth.

4. Conclusion

This paper investigated the problem of focusing the out-of-plane velocity component on the surface of an isotropic solid sample. The numerical model used in the analysis was first validated against experimental data. Subsequently, empirical expressions for the width and depth of the focal spot (that of the out-of-plane velocity component) were found based on (i) an interpretation of Lamb's problem to determine which waves dominate the propagation in the regions of interest (surface and bulk) and (ii) the use of the diffraction limit. In these expressions: the width of the focal spot depends only on the wavelength of the Rayleigh wave and the depth on the wavelength of the shear wave, at the center frequency of the focused pulse. The empirical expressions were found to be robust to changes of the center frequency of the focused pulse and of the Poisson's ratio of the material. The problem studied in this paper is of interest in a number of NDT applications. In the experiments conducted recently by the authors [7], it is now sufficient to measure the size of the TR focal spot on the surface of the sample to infer how deep the sample is probed.

Acknowledgment

This work was funded by the U.S. Dept. of Energy, Fuel Cycle R&D, Used Fuel Disposition (Storage) campaign.

References

- [1] T.J. Ulrich, P.A. Johnson, R.A. Guyer, Interaction dynamics of elastic waves with a complex nonlinear scatterer through the use of a time reversal mirror, *Phys. Rev. Lett.* 98 (2007) 104301.
- [2] T.J. Ulrich, A.M. Sutin, T. Claytor, P. Papin, P.-Y. Le Bas, J.A. Ten Cate, The time reversed elastic nonlinearity diagnostic applied to evaluation of diffusion bonds, *Appl. Phys. Lett.* 93 (2008) 151914.
- [3] T.J. Ulrich, A.M. Sutin, R.A. Guyer, P.A. Johnson, Time reversal and non-linear elastic wave spectroscopy (TR NEWS) techniques, *Int. J. Non-Linear Mech.* 43 (2008) 209–216.
- [4] O. Bou Matar, S. Dos Santos, J. Fortineau, T. Goursolle, L. Haumesser, and F. Vander Meulen, Pseudo spectral simulations of elastic waves propagation in heterogeneous nonlinear hysteretic medium, in: Proceedings of the 17th International Symposium of Nonlinear Acoustics, State College, PA, 2005, pp. 95–98.

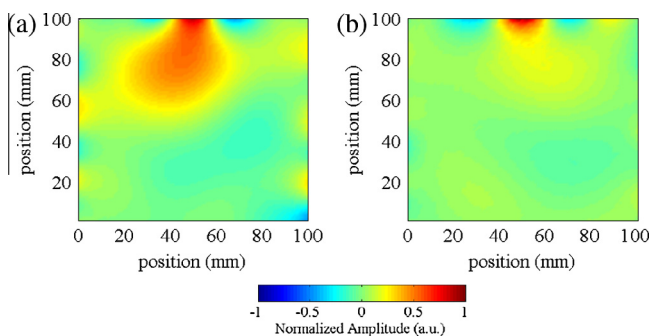


Fig. 8. Simulated volumetric strain fields at the focal time with (a) 2D and (b) 3D models. In 3D, a slice of the data is extracted in the x - z plane, following the cut depicted in Fig. 4. Due to symmetry, identical results are obtained in the y - z plane. Focusing was achieved using the v_z component. A Ricker wavelet centered at 75 kHz was used in the *forward-propagation* problem.

- [5] G. Zumpano, M. Meo, A new nonlinear elastic time reversal acoustic method for the identification and localisation of stress corrosion cracking in welded plate-like structures – a simulation study, *Int. J. Solids Struct.* 44 (2007) 3666–3684.
- [6] T. Goursole, S. Callé, S. Dos Santos, O. Bou Matar, A two-dimensional pseudospectral model for time reversal and nonlinear elastic wave spectroscopy, *J. Acoust. Soc. Am.* 122 (2007) 3220–3229.
- [7] C. Payan, T.J. Ulrich, P.Y. Le Bas, M. Griffa, P. Schuetz, M.C. Remillieux, T.A. Saleh, Probing material nonlinearity at various depths by time reversal mirrors, *Appl. Phys. Lett.* 104 (2014) 144102.
- [8] B.E. Anderson, M. Griffa, C. Larmat, T.J. Ulrich, P.A. Johnson, Time reversal, *Acoust. Today* 4 (2008) 5–16.
- [9] M. Fink, Time reversal of ultrasonic fields – Part I: basic principles, *IEEE Trans. Ultrason. Ferroelectr. Freq. Contr.* 39 (1992) 555–566.
- [10] A. Parvulescu, C.S. Clay, Reproducibility of signal transmission in the ocean, *Radio Electr. Eng.* 29 (1965) 223–228.
- [11] C. Draeger, J.-C. Aime, M. Fink, One-channel time-reversal in chaotic cavities: experimental results, *J. Acoust. Soc. Am.* 105 (1999) 618–625.
- [12] A. Sutin, J.A. TenCate, P.A. Johnson, Single-channel time reversal in elastic solids, *J. Acoust. Soc. Am.* 116 (2004) 2779–2784.
- [13] J.D. Achenbach, *Reciprocity in Elastodynamics*, Cambridge University Press, Cambridge, UK, 2003.
- [14] D. Cassereau, M. Fink, Time-reversal of ultrasonic fields. Part III: theory of the closed time-reversal cavity, *IEEE Trans. Ultrason. Ferroelectr. Freq. Contr.* 39 (1992) 579–592.
- [15] A. Derode, P. Roux, M. Fink, Robust acoustic time reversal with high-order multiple scattering, *Phys. Rev. Lett.* 75 (1995) 4206–4209.
- [16] C. Draeger, M. Fink, One-channel time-reversal in chaotic cavities: theoretical limits, *J. Acoust. Soc. Am.* 105 (1999) 611–617.
- [17] C. Draeger, J.-C. Aime, M. Fink, One-channel time reversal in chaotic cavities: experimental results, *J. Acoust. Soc. Am.* 105 (1999) 618–625.
- [18] O. Bou Matar, Y.F. Li, K. Van Den Abeele, On the use of a chaotic cavity transducer in nonlinear elastic imaging, *Appl. Phys. Lett.* 95 (2009) 141913.
- [19] C. Draeger, D. Cassereau, M. Fink, Theory of the time-reversal process in solids, *J. Acoust. Soc. Am.* 102 (1997) 1289–1295.
- [20] C. Draeger, D. Cassereau, M. Fink, Acoustic time reversal with mode conversion at a solid–fluid interface, *Appl. Phys. Lett.* 72 (1998) 1567–1569.
- [21] T.J. Ulrich, K. Van Den Abeele, P.-Y. Le Bas, M. Griffa, B.E. Anderson, R.A. Guyer, Three component time reversal: focusing vector components using a scalar source, *J. Appl. Phys.* 106 (2009) 113504.
- [22] T. Goursole, S. Dos Santos, O. Bou Matar, S. Calle, A two-dimensional pseudospectral model for time reversal and nonlinear elastic wave spectroscopy, *J. Acoust. Soc. Am.* 122 (2007) 3220–3229.
- [23] E.N. Jansen, K. Van Den Abeele, Dual energy time reversed elastic wave propagation and nonlinear signal processing for localisation and depth-profiling of near-surface defects: a simulation study, *Ultrasonics* 51 (2011) 1036–1043.
- [24] F. Simonetti, P. Cawley, A guided wave technique for the characterization of highly attenuative viscoelastic materials, *J. Acoust. Soc. Am.* 114 (1) (2003) 158–165.
- [25] H. Lamb, On the propagation of tremors over the surface of an elastic solid, *Philos. Trans. R. Soc. Lond.* A203 (1904) 1–42.
- [26] G.F. Miller, H. Pursey, The field and radiation impedance of mechanical radiators on the free surface of a semi-infinite isotropic solid, *Philos. Trans. R. Soc. Lond.* A233 (1944) 521–541.
- [27] J.D. Achenbach, *Wave Propagation in Elastic Solids*, Elsevier Science, Amsterdam, 1973.